Centrum voor Wiskunde en Informatica
REPORT*RAPPORT*

An analysis of crystal dissolution fronts in flows through porous media Part 2: Incompatible boundary conditions

C.J. van Duijn, P. Knabner, R.J. Schotting

Department of Analysis, Algebra and Geometry

AM-R9609 July 31, 1996

Report AM-R9609
ISSN 0924-2953

CWI
P.O. Box 94079
1090 GB Amsterdam
The Netherlands

An Analysis of Crystal Dissolution Fronts in Flows through Porous Media
Part 2: Incompatible Boundary Conditions

C. J. van Duijn
CWI,
P.O. Box 94079, 1090 GB Amsterdam, The Netherlands
email: hansd@cwi.nl

P. Knabner
University of Erlangen–Nürnberg, Institute of Applied Mathematics,
Martensstraße 3, D – 91058 Erlangen, Germany
email: knabner@am.uni-erlangen.de

R.J. Schotting[1]
CWI,
P.O. Box 94079, 1090 GB Amsterdam, The Netherlands
email: ruuds@cwi.nl

Abstract

A model for transport of solutes in a porous medium participating in a dissolution/precipitation reaction, in general not in equilibrium, is studied. Ignoring diffusion/dispersion the initial value problem for piecewise constant initial states is studied, which e.g. for ionic species include a change of the ionic composition of the solution. The mathematical solution, nearly explicitly found by the method of characteristics up to the (numerical) solution of an integral equation for the position of the dissolution front, exhibit a generalized expanding plateau-structure determined by the dissolution front and the water flow (or salinity) front.

AMS Subject classification: 35R35, 76S05
Key words & Phrases: Transport, travelling wave, crystal dissolution, porous media, mathematical analysis.

1 Introduction

In this paper we continue our study of chemistry affected transport processes in porous media from Knabner et.al. [3], here after referred to as Part 1. The transported solutes are participants in a precipitation-dissolution reaction, which in general is not in equilibrium, but is kinetically controlled. In Part 1 we have set up a model which for spatially one-dimensional flow regimes with constant water content, bulk density, pore velocity q [cm/s] and diffusion/dispersion coefficient D [cm^2/s] reads as follows: The unknown functions u and v [mM/cm^3], u being the molar concentration of one of the reacting participants in solution, v being the scaled concentration of the crystalline solid, both relative to the water volume, and a third unknown w [-], which appears to take into account the nature of the dissolution reaction, have to satisfy the equations

$$\frac{\partial}{\partial t}(u+v) + q\frac{\partial u}{\partial x} - D\frac{\partial^2 u}{\partial x^2} = 0 \tag{1}$$

$$\frac{\partial v}{\partial t} = k\{g(u;c) - wK\} \tag{2}$$

$$0 \le w \le 1 \quad \text{and} \quad w(x,t) = 1 \quad \text{if} \quad v(x,t) > 0 \tag{3}$$

[1] Note: Corresponding author.

for $-\infty < x < \infty$, $t > 0$. The positive constants K, k are the saturation constant and a rate parameter, respectively. There is a further function c in the nonlinear function g related to the precipitation reaction. It is a conserved quantity in the sense that it satisfies the linear diffusion-advection equation

$$\frac{\partial c}{\partial t} + q\frac{\partial c}{\partial x} - D\frac{\partial^2 c}{\partial x^2} = 0 \tag{4}$$

for $-\infty < x < \infty$, $t > 0$. The function c is solely determined by the stoichiometry of the precipitation-dissolution reaction. If this is given by

$$\overline{M}_{12} \rightleftharpoons nM_1 + mM_2 \tag{5}$$

with positive integers n, m where M_1, M_2 denote the species in solution and $\overline{M}_{12}$ the solid, then

$$c = mc_1 - nc_2 \tag{6}$$

and c_1, c_2 [mM/cm^2] are the molar concentrations of M_1, M_2. In (1)-(4), $c_1 = u$ is kept as an unknown and c_2 is substituted by means of (6). For a spatially independent batch situation the function c would be constant due to (4), i.e. all possible values of concentrations $c_1(t), c_2(t)$ lie in an affine subspace of the one-dimensional stoichiometric subspace of the reaction, defined by the condition $c = 0$. In the case of ionic species, it is also possible to consider c as the scaled total (positive) electric charge of the solution. This observation helps us in distinguishing two principal situations with respect to a specification by means of initial conditions. We will consider piecewise constant states at $t = 0$, i.e.

$$u(x,0), v(x,0), c(x,0) = \begin{cases} u^*, v^*, c^* & \text{for} \quad x < 0 \\ u_*, v_*, c_* & \text{for} \quad x > 0 \end{cases} \tag{7}$$

We can relate these solutions to solutions of a corresponding boundary value problem for $x > 0, t > 0$ by considering u_*, v_*, c_* as initial conditions and u^*, v^*, c^* as boundary conditions. Thus there are two situations

$$c^* = c_* \text{ and therefore } c(x,t) = c = \text{constant} \tag{8}$$

or

$$c^* \neq c_* \tag{9}$$

In case (8) the boundary(/initial) conditions are compatible in the sense that they belong to the same affine stoichiometric subspace of the reaction or for ionic species that the injected fluid has the same ionic composition as the resident fluid. This situation is the only one which leads to travelling wave solutions being the subject of Part 1. Here we concentrate on case (9), i.e. on incompatible boundary(/initial) conditions. In this paper we show how to obtain solutions of this problem in the presence of a dissolution front, i.e. a curve in the (x,t)-plane separating the region where $v = 0$ from the region where $v > 0$. To ensure that a dissolution front exists for all $t \geq 0$, one needs

$$v^* = 0 \quad \text{and} \quad v_* > 0. \tag{10}$$

If initially crystalline solid is everywhere present in the flow domain, i.e. $v^* > 0$ as well, then a dissolution front may occur after a certain finite time interval. Conditions for which this happens are discussed in Section 3.2.
A typical example for the function g is, assuming the thermodynamically ideal mass action law:

$$g(u;c) = u^n \left(\frac{1}{n}(mu - c)\right)^m \tag{11}$$

where (6) is used and thus only the variable $u \geq (c/m)_+$, where $a_+ = a$ for $a \geq u$, $a_+ = 0$ for $a < 0$, is allowed to insure $c_1 \geq 0$, $c_2 \geq 0$. In general the function g has the following properties to be used later on:

$g(\cdot;c)$ is strictly monotone increasing for $u \geq (c/m)_+$,

$g(\cdot;c)$ is smooth for $u \geq (c/m)_+$ (at least Lipschitz-continuous).

We need the existence of a (unique) $u_S = u_S(c) \geq (c/m)_+$ such that

$$g(u;c) = K \tag{12}$$

i.e. u_S is the solubility for given c. Due to the properties of the function g given above, the following condition fulfilled by (11) is sufficient for (12):

$$g\left(\left(\frac{c}{m}\right)_+ ; c\right) = 0. \tag{13}$$

When we require (10), we additionally assume the initial states to be in chemical equilibrium, i.e.

$$\left(\frac{c}{m}\right)_+ \leq u^* \leq u_S(c^*) \quad \text{and} \quad u_* = u_S(c_*). \tag{14}$$

If solid is present everywhere, this would not lead to the appearance of a dissolution front (see 66),(67)), thus we allow in this case for an initial state for $x < 0$ not in equilibrium, which might be thought of as the consequence of an instantaneous removal of saturated fluid.
If dispersive transport is negligible compared to the advective transport, it is reasonable to let $D \to 0$, i.e. to cancel the corresponding terms in (1)-(4) and to obtain

$$\frac{\partial}{\partial t}(u+v) + q\frac{\partial u}{\partial x} = 0 \tag{15}$$

$$\frac{\partial v}{\partial t} = k\{g(u;c) - wK\} \tag{16}$$

$$0 \leq w \leq 1 \quad \text{and} \quad w(x,t) = 1 \quad \text{if} \quad v(x,t) > 0 \tag{17}$$

$$\frac{\partial c}{\partial t} + q\frac{\partial c}{\partial x} = 0 \tag{18}$$

for $-\infty < x < \infty$, $t > 0$. The initial value problem (15)–(18) and (7) is known as a Riemann problem. In this paper we consider the analytical and numerical construction of a solution of this Riemann problem. For dominating advective transport we expect a good approximation of the solutions of (1)–(4) and (7) ignoring only certain smoothing effects (see the comparison in Section 5). On the other hand, the treatment of the hyperbolic system by means of the method of characteristics allows a nearly explicit construction of the solution and thus gives detailed information about the qualitative structure of the solution. The function c is found directly, without apriori knowledge about u, v and w. It follows from (18) and (7) that for all $t \geq 0$

$$c(x,t) = \begin{cases} c^* & \text{for} \quad x < q\,t, \\ c_* & \text{for} \quad x > q\,t. \end{cases} \tag{19}$$

To be specific, we assume in the following

$$c^* > c_*. \tag{20}$$

The other case can be treated in exactly the same way or transformed to the above situation, which basically corresponds to a renumbering of the dissolved reaction participants. A further property, which holds true for the example (11), is the monotone dependence of the solubility $u_S(c)$ on c, i.e. in particular

$$u_S(c^*) > u_S(c_*). \tag{21}$$

In the analysis we will not make use of this property, but in the figures it is assumed to hold true or implied by the choice of example (11). The outline of the paper is as follows: We first construct a solution of the Riemann problem in the case of equilibrium reactions. That is, we take '$k = \infty$' in equation (16) and replace it by

$$g(u;c) = w\,K. \tag{22}$$

In Section 3.1 we use the method of characteristics, which leads to an explicit representation of the solution, but still dependent on the dissolution front $x = s(t)$. For this free boundary, which necessarily exhibits a waiting time (55), we derive an integral equation (DFE) ((61)), which in Section 4 can be transformed to a linear Volterra equation of the second kind, due to various properties of solution. This settles the existence of a solution of (DFE), which then can be used to define a solution of the Riemann problem. In Section 3.2 this procedure is extended to the treatment of $v_*, v^* > 0, u^* \leq u_S(c^*)$. In Section 5 an algorithm for the precise approximation of solutions is modelled according to the above procedure. The analysis of multi component reactive systems with pure advective transport by means of the corresponding hyperbolic systems has a certain tradition in the chemical engineering literature. Although the situation considered usually allows for more species and reactions as considered here, most of these papers have to restrict themselves to equilibrium reactions and a constant number of phases (see e.g. Schweich et.al. [5] and the literature cited there). The simple situation studied in this paper is just characterized by the opposite by non-equilibrium and the appearance of a dissolution front.

2 Equilibrium

When studying the transport process at equilibrium we replace the first order equation (16) by the equilibrium relation (22). Thus the equations to be analyzed are

$$\frac{\partial(u+v)}{\partial t} + q\frac{\partial u}{\partial x} = 0 \tag{23}$$

$$g(u;c) = wK \tag{24}$$

$$0 \leq w \leq 1 \text{ and } w(x,t) = 1 \text{ if } v(x,t) > 0, \tag{25}$$

where c is given by (19). In this section we construct a solution of this system in the domain $-\infty < x < +\infty$ for $t > 0$, which satisfies at $t = 0$ the piecewise constant initial distribution (7). We recall that the constant states in (7) fulfill conditions (14). To emphasize the role of the dissolution front we impose condition (10) as well. This simple case is treated for further comparison and introduction of the techniques to be used. In fact the result of this section is well-known in the chemical engineering literature (at least formally) and a special case of e.g. Bryant et.al. [1].
For the construction, the following two observations are essential. The first one relates to equation (24) and says that if $v(x,t) > 0$ then $w(x,t) = 1$ and by (24)

$$g(u(x,t); c(x,t)) = K \tag{26}$$

In addition, if $x > qt$ then $u(x,t) = u_S(c_*) = u_*$ and if $x < qt$ then $u(x,t) = u_S(c^*)$.
The second one is the Rankine-Hugoniot shock condition for solutions of (23). This condition which is based on a mass-conservation argument (see for instance Whitham [7] or LeVeque [4], says that discontinuities or shocks in solutions of equation (23) propagate with

$$\text{speed} \quad = \frac{[u]}{[u+v]}\, q. \tag{27}$$

Here the quantities between the brackets denote the size of the jump discontinuity in u and v across the location of the shock.

Now suppose a dissolution front $x = s(t)$ exists such that

$$v(x,t) = \begin{cases} 0 \text{ for } & x < s(t) \\ > 0 \text{ for } & x > s(t). \end{cases} \tag{28}$$

On physical grounds one expects $s(t) \leq qt$ for all $t > 0$, because q denotes the averaged pore velocity of the fluid: i.e. ahead of the front $x = qt$ one expects to find the initial states $u = u_*$ and $v = v_*$.

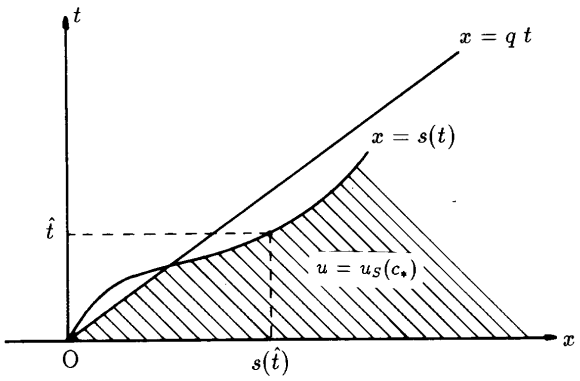

Fig 1. Dissolution front ahead of the fluid front.

The mathematical argument is the following. Suppose the dissolution front moves ahead of the fluid front, as in Figure 1. Since $w(x,t) = 1$ for $x > s(t)$ we find from (26) that $u = u_S(c_*)$ in the shaded region in Figure 1. Next select $\hat{t} > 0$ such that

$$s(\hat{t}) > q\hat{t} \text{ and } \dot{s}(\hat{t}) > q, \tag{29}$$

where the dot denotes differentiation. In other words, we have selected a time $\hat{t}$ at which the speed of the dissolution front exceeds q. Then by the Rankine-Hugoniot condition (27),

$$u(s(\hat{t})^-, \hat{t}) > u_* = u_S(c_*), \tag{30}$$

as v jumps downwards from right to left or does not jump. Here $u(y^-,t) = \lim_{x\uparrow y} u(x,t)$ denotes the limit in y from the left and $u(y^+,t) = \lim_{x\downarrow y} u(x,t)$ the limit from the right. But $c(s(\hat{t}),\hat{t}) = c_*$, and thus by (24) and (25)

$$u(s(\hat{t})^-, \hat{t}) \leq u_S(c_*), \tag{31}$$

a contradiction. In other words, assumption (29) implies over-saturation for u. But this is not allowed under equilibrium conditions. We further note that if v is discontinuous at the dissolution front, i.e. $v(s(t)^+,t) > 0$ then $\dot{s}(t) = q$ cannot occur. This is a direct consequence of (27). This observation implies that $s(\hat{t}) = q\hat{t}$ and $\dot{s}(\hat{t}) = q$ for some $\hat{t} > 0$ can also not occur as $v(s(\hat{t})^+,\hat{t}) = v_* > 0$. Hence

$$s(t) < qt \text{ for all } t > 0. \tag{32}$$

The ordering of the fronts and (24),(26) imply

$$u(x,t) = \begin{cases} \leq u_S(c^*) & -\infty < x < s(t) \\ u_S(c^*) & s(t) < x < qt \\ u_S(c_*) & qt < x < +\infty \end{cases} \tag{33}$$

Consequently by (27)

$$0 \leq \dot{s}(t) \leq q \text{ for all } t > 0 \tag{34}$$

and $\dot{s}(\hat{t}) < q$ occurs at points $\hat{t}$ where v is discontinuous. In particular this shows that all dissolution fronts are monotone in time. Since v vanishes in the region $x < s(t)$, we have there

$$\frac{\partial u}{\partial t} + q\frac{\partial u}{\partial x} = 0. \tag{35}$$

The initial condition on u for $x < 0$, the upperbound in (34) and equation (35) imply that $u = u^*$ for $x < s(t)$. To determine v in the region $x > s(t)$ we use (33) and equation (23). Combined they imply that $\partial v(x,t)/\partial t = 0$ for $x > s(t)$, $x \neq qt$. Then using the initial condition on v for $x > 0$ and the lower bound on $\dot{s}$, we find after integration $v = v_*$ for $x > s(t)$. Thus we have constructed a piecewise constant solution of (23)-(25) which satisfies the initial distribution (7). The dissolution front follows from the Rankine-Hugoniot condition (27): $s(t) = at$, with

$$a = \frac{u_S(c^*) - u^*}{u_S(c^*) - u^* + v_*}\, q \quad (< q) \tag{36}$$

Across the other shock, $x = qt$, v is constant. This is consistent with (27). In the chemical engineering literature this front is called the salinity front. (see e.g. Bryant et.al. [1]) In Figure 2 we show the level set of the solution $\{u, v, w, c\}$ at equilibrium. The separating curves are shock curves at $x = at$ and $x = qt$. Figure 3 shows a sketch of the profiles of the variables for some $t > 0$. A detailed comparison

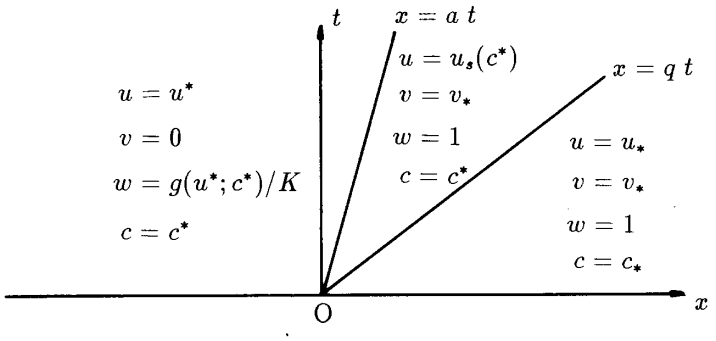

Fig 2. Level sets of concentrations at equilibrium.

with the computations of Willis and Rubin [6] will be given in Section 5.

One may raise the question if the solution as constructed in this section is the unique solution of the initial value problem. For the following reasons we believe that it is. In the construction, inequalities (34) are crucial. They imply directly that the concentrations u and v are constant to the left and the right of a dissolution front, leading to the constant speed (36). In (34) the inequalities are a consequence of the Rankine-Hugoniot condition and the fact that over-saturation is ruled out by requiring $w \leq 1$ in (25). In other words, (34) are local properties of any dissolution front. As outlined above they lead to a piecewise constant solution as presented in this section.

3 Non-equilibrium

When precipitation-dissolution reactions cannot assumed to be at equilibrium, one needs to incorporate the first-order reaction equation (16) in the description. This leads to a much more involved analysis. In this section we construct solutions of the Riemann problem (15)-(18) and (7) for two distinct cases. In Section 3.1 we assume (10) to be satisfied, implying that crystalline solid is present only in part of the flow domain, and in Section 3.2 we assume $v^*, v_* > 0$. In this first case a dissolution front exists for all $t \geq 0$. In the second case it may appear in finite time.

3.1 Crystalline solid partly present

Inspired by the '$k = \infty$' results, we start with the assumption that a dissolution front exists, as in (28), which satisfies inequalities (34). These inequalities are crucial for the construction of a solution.

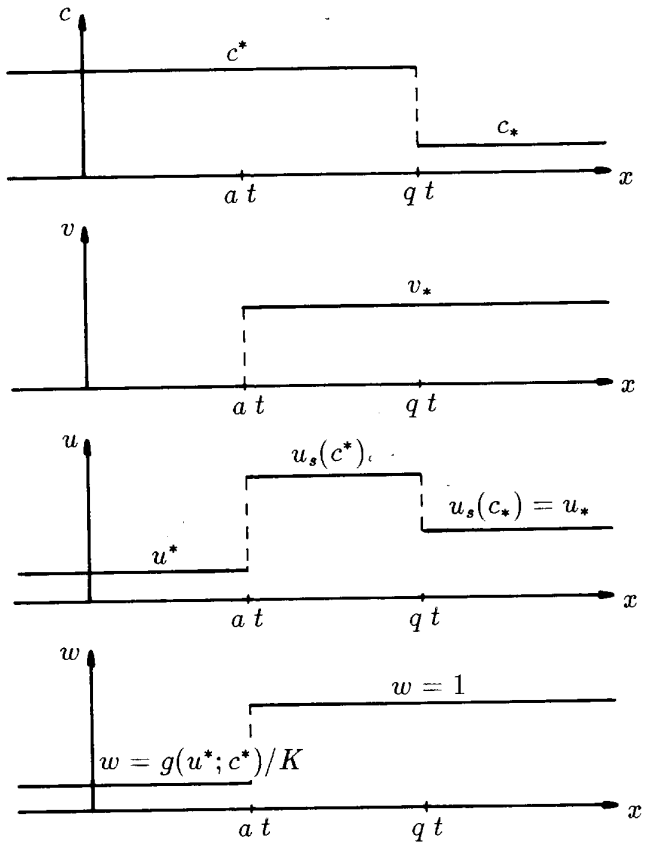

Fig 3. Sketch of profiles at some $t > 0$.

Unfortunately there are no obvious physical or mathematical arguments to support these assumptions. In contrast, the weaker statement $s(t) \leq qt$ for all $t \geq 0$, which is obviously physical, can be justified similarly as in Section 2. We return to the possibility of existence of solutions not fulfilling these assumptions when discussing the uniqueness at the end of Section 4. The main goal is to derive an equation for the location $x = s(t)$ of the dissolution front.

As in Section 2 we conclude, because of $\frac{\partial v}{\partial t} = 0$ for $x < s(t)$, that $u = \text{const} = u^*$ for $x < s(t)$ and that $w = g(u^*, c^*)/K$ there. Similarly for $x > qt$ we have $u = \text{const} = u_* = u_S(c_*)$ and thus $v = \text{const} = v_*$. With reference to Figure 4, we are going to consider the following problem:

Find a u, v and s such that

$$\begin{aligned} \frac{\partial u}{\partial t} + q\frac{\partial u}{\partial x} &= k\{K - g(u; c^*)\} \\ & \qquad \text{for } s(t) < x < qt \text{ and for } t > 0 \\ \frac{\partial v}{\partial t} &= k\{g(u; c^*) - K\} \end{aligned} \tag{37}$$

such that

$$u(s(t), t) = u^*, \; v(s(t), t) = 0 \tag{38}$$

and

$$v(qt, t) = v_* \tag{39}$$

Note that in the composite solution the crystalline concentration v is continuous across $x = qt$, due to (27) and then (39) holds, while the fluid concentration u possibly has a discontinuity there.

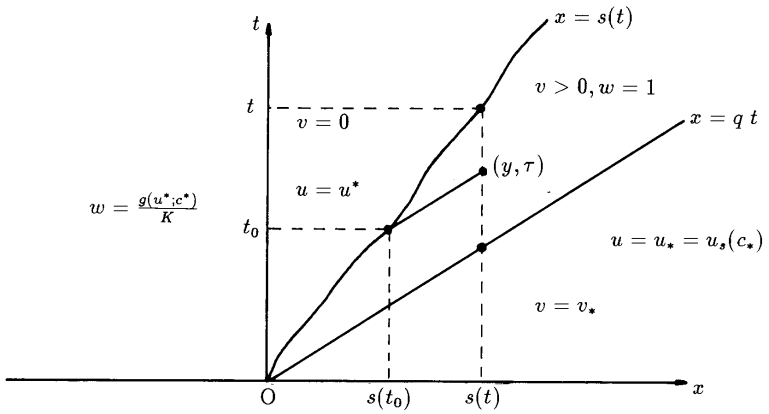

Fig 4. Dissolution front in the (x,t)-plane.

We solve equation (37) by the method of characteristics. Choose any point (y,τ) in the domain $\{(x,t) : s(t) < x < qt, t > 0\}$, see also Figure 4. The characteristics of (37) are straight lines in the (x,t)-plane having slope q with respect to the t-axis. The characteristic passing through the point (y,τ), i.e. the curve $x = y + q(t-\tau)$, intersects the dissolution front in the point $(s(t_0), t_0)$, which satisfies

$$s(t_0) = y + q(t_0 - \tau). \tag{40}$$

Due to $\dot{s}(t) \leq q$ this point is unique and thus is the same for all starting points (y,τ) satisfying (40). For a given dissolution front $s(t)$, this would determine t_0 as a function of y and τ, i.e. $t_0 = t_0(y,\tau)$. Integrating (37) along the characteristic and using the first condition in (40) yields

$$\int_{u^*}^{u(y,\tau)} \frac{1}{k\{K - g(z;c^*)\}}\, dz = \tau - t_0(y,\tau) = \frac{y - s(t_0(y,\tau))}{q} \tag{41}$$

The idea is now to use equation (37) and the boundary conditions on v to determine the location of the dissolution front, i.e. to find the function $s(t)$. Before we proceed we first introduce for the case $u^* < u_S(c^*)$ the function $f : [0,+\infty) \to [u^*, u_S(c^*))$ defined implicitly by the integral

$$\int_{u^*}^{f(\delta)} \frac{1}{k\{K - g(z;c^*)\}}\, dz = \frac{\delta}{q} \quad \text{for all } \delta \geq 0, \tag{42}$$

and the function $F : [0,+\infty) \to (0,+\infty)$, defined by

$$F(\delta) = k\{K - g(f(\delta);c^*)\} \quad \text{for all } \delta \geq 0. \tag{43}$$

Note that due to the differentiability of $g(\cdot;c^*)$ at $u = u_S(c^*)$

$$\int_{u^*}^{u} \frac{1}{k\{K - g(z;c^*)\}}\, dz \to \infty \quad \text{for } u \to u_S(c^*) \tag{44}$$

and thus f and F are well defined.

Examples. Let the rate function g be given by the law of mass action (11). We can explicitly compute the cases:

n=1,m=0 (The linear case, see also Part I, equation (40)).
Then $g(u;c) = u$ and $u_S(c) = K$, independent of c. We find

$$f(\delta) = K - (K - u^*)e^{-\frac{k}{q}\delta} \tag{45}$$

and

$$F(\delta) = k(K - u^*)e^{-\frac{k}{q}\delta} \tag{46}$$

n=1,m=1. (See Figure 5).
Then $g(u;c) = u(u-c)$ and $u_S(c) = \frac{c}{2} + \frac{1}{2}\sqrt{c^2 + 4K}$. We find that f satisfies

$$\frac{f(\delta) - u_0}{u_S - f(\delta)} = \frac{u^* - u_0}{u_S - u^*}e^{\alpha\delta} \tag{47}$$

where $u_S = u_S(c), u_0 = u_0(c) = \frac{c}{2} - \frac{1}{2}\sqrt{c^2 + 4K}$ and $\alpha = \frac{k}{q}(u_S - u_0)$. Consequently

$$F(\delta) = k(u_S - u_0)^2 \frac{u^* - u_0}{u_S - u^*} \frac{e^{-\alpha\delta}}{\{e^{-\alpha\delta} + \frac{u^* - u_0}{u_S - u^*}\}^2} \tag{48}$$

When $u^* = u_S(c^*)$, which we consider as a degenerate case, we extend the definitions (42) and (43) by

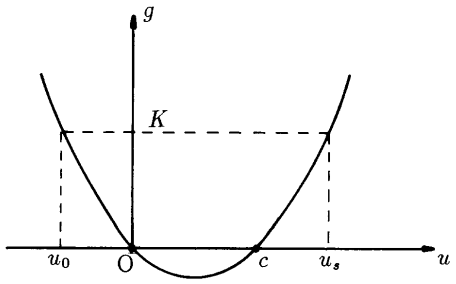

Fig 5. Rate function g for $n = m = 1$. Note that $u^* \geq c$.

setting

$$f(\delta) = u_S(c^*) \text{ and } F(\delta) = 0 \text{ for all } \delta \geq 0. \tag{49}$$

Unless stated otherwise we avoid this degeneracy by taking $u^* < u_S(c^*)$. This implies $F(\delta) > 0$ and $F'(\delta) < 0$ for all $\delta \geq 0$.

Next we continue the analysis of (41). Take any $t > 0$ and let $y = s(t)$. Using definitions (42),(43) we now write

$$k\{K - g(u(s(t), \tau); c^*)\} = F(s(t) - s(t_0)), \tag{50}$$

for any $s(t)/q < \tau < t$. Here we have used $\dot{s}(t) \geq 0$. In this expression, $t_0 = t_0(s(t), \tau)$ satisfies $t_0 = t$ when $\tau = t$. Substituting (50) into the rate equation (37), integrating the result and applying the v-boundary condition in (38) and (39), yields

$$\int_{\frac{s(t)}{q}}^{t} F(s(t) - s(t_0))\, d\tau = v_*. \tag{51}$$

Remind that in deriving this equation we in particular assumed s to be monotone, but not to be strictly monotone. In the derivation of (51) we can allow for constant parts of s, i.e. for times $0 \leq t_1 < t_2$ such

that $s(t) = s(t_1)$ for all $t_1 \leq t \leq t_2$. In such a case the definition of $t_0 = t_0(s(t), \tau)$ gives for t such that $t_1 \leq t \leq t_2$:

$$t_0(s(t), \tau) = \tau \text{ for } \tau \in [t_1, t] \tag{52}$$

and the whole derivation of equation (51) holds true with the following exception: If $s(t) = 0$ for $0 \leq t \leq t_2$, then the integration leading to (51) cannot be performed for $t \in [0, t_2]$ as $v(0,0)$ is not defined. But on the other hand a dissolution front as sketched in Figure 4, i.e. $s(0) = 0$ and $s(t) > 0$ for $t > 0$, would lead to a contradiction in (51). Letting $t \downarrow 0$ would make the left hand side zero while $v_* > 0$ as given. Therefore we have a waiting time $t_* > 0$, see Figure 6, such that

$$s(t) = \begin{cases} 0 & \text{for } 0 \leq t \leq t_*, \\ > 0 & \text{for } t > t_*. \end{cases} \tag{53}$$

From equation (51) for $t \downarrow t_*$ we conclude

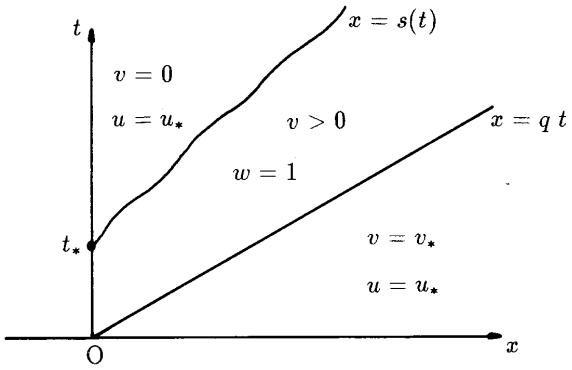

Fig 6. Waiting time in dissolution front.

$$t_* F(0) = v_*. \tag{54}$$

Using (42) and (43) we find for the waiting time the expression

$$t_* = \frac{v_*}{k\{K - g(u^*, c^*)\}}. \tag{55}$$

Note that in the degenerate case $u^* = u_S(c^*)$ expression (55) implies $t_* = \infty$. In other words, when u^* equals the solubility concentration then the dissolution front remains stagnant. Further more, apart from the initial waiting time, no further constant parts of s can occur: if this would be the case, say on the interval $[t_1, t_2]$, then we can conclude from (51)

$$\begin{aligned} v_* &= \int_{s(t_2)/q}^{t_2} F(s(t_2) - s(t_0))\, d\tau \\ &= \int_{t_1}^{t_2} F(s(t_1) - s(t_0))\, d\tau + \int_{s(t_1)/q}^{t_1} F(s(t_1) - s(t_0))\, d\tau \\ &= \int_{t_1}^{t_2} F(0)\, d\tau + v_*, \end{aligned} \tag{56}$$

which is a contradiction. We want to rewrite the integral in (51) in terms of t_0 and we do this by using (40). From that equality, with $y = s(t)$, we obtain due to $\dot{s}(t) \leq q$ a unique correspondence of the points τ with the points t_0, where

$$\tau : \frac{s(t)}{q} \to t \text{ implies } t_0 : 0 \to t \tag{57}$$

and

$$\frac{\partial \tau}{\partial t_0} = 1 - \frac{1}{q}\dot{s}(t_0). \tag{58}$$

Applying these observations to (51) yields

$$\begin{aligned}\int_0^t F(s(t) - s(t_0))\, dt_0 &= v_* + \frac{1}{q}\int_0^t F(s(t) - s(t_0))\dot{s}(t_0)\, dt_0 \\ &= v_* + \frac{1}{q}\int_0^{s(t)} F(z)\, dz,\end{aligned} \tag{59}$$

where the left-hand side can be slightly rewritten by introducing the waiting time:

$$\int_0^t F(s(t) - s(t_0))\, dt_0 = t_* F(s(t)) + \int_{t_*}^t F(s(t) - s(t_0))\, dt_0. \tag{60}$$

To summarize, we have obtained an integral equation from which the location of the dissolution front can be determined. The precise formulation is: Let t_* be given by (55). Then find the function $s(t)$, satisfying (53) and the dissolution front equation (DFE)

$$(DFE)\begin{cases} \displaystyle\int_{t_*}^t F(s(t) - s(t_0))\, dt_0 = B(s(t)) \text{ for } t \geq t_* \text{ where} \\ B(s(t)) := t_*\{F(0) - F(s(t))\} + \frac{1}{q}\displaystyle\int_0^{s(t)} F(z)\, dz. \end{cases} \tag{61}$$

The expression for B follows from (54),(59) and (60). In general we have to rely on numerical methods to solve (DFE). One such method will be discussed in Section 5. Only very special cases can be solved analytically, for instance the case $n = 1$ and $m = 0$ (the linear case) in the examples, where F is give by (46). For that form of F it is straight forward to solve (DFE) explicitly. The result is

$$s(t) = \frac{q}{1 + kt_*}(t - t_*) \text{ for } t \geq t_*, \tag{62}$$

where

$$t_* = \frac{v_*}{k(K - u^*)}. \tag{63}$$

In Section 4 we show how to transform (DFE) into a standard integral equation, from which some characteristic properties of the front can be derived. Having found an expression or approximation for $s(t)$, one has to go back to equation (41) and definition (42) to determine u. The concentration of the crystalline solid is obtained from integrating (37).

3.2 Crystalline solid everywhere present

As in the previous case, the concentrations ahead of the fluid front are not affected by the displacing fluid and therefore equal to the initial concentrations. Since v is continuous across $x = qt$, the essential parameters which determine the behavior of the concentrations are u^*, v^*, c^* (rather $u_S(c^*)$) and v_*, see Figure 7. For definiteness we assume here that $v^* < v_*$. As long as $v > 0$, implying $w = 1$, we need to

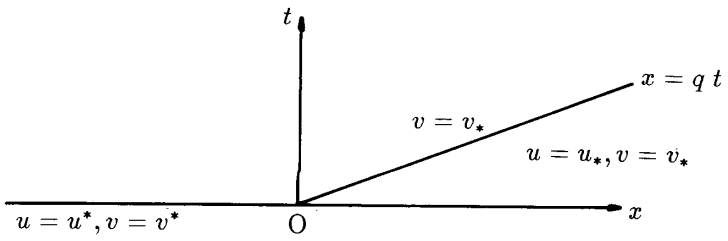

Fig 7. Initial conditions for the domain $x < qt, t > 0$.

solve equations (37),(37) subject to the conditions shown in Figure 7. Integrating the u-equation along the characteristic $x - qt =$ constant and the v-equation in t, we find that

$$u(x,t) = f(qt) \quad \text{for} \quad x < 0 \quad \text{or} \quad 0 < x < qt \quad \text{and} \quad t > 0, \tag{64}$$

with f defined by (42) and

$$v(x,t) = \begin{cases} v^* + u^* - f(qt) & \text{for} \quad x < 0, \quad t > 0 \\ v_* + f(x) - f(qt) & \text{for} \quad 0 < x < qt, \quad t > 0 \end{cases} \tag{65}$$

Note that f is monotonically increasing from $f(0) = u^*$ towards $f(\infty) = u_S(c^*)$. The crystalline solid concentration for fixed $t > 0$ is sketched in Figure 8.

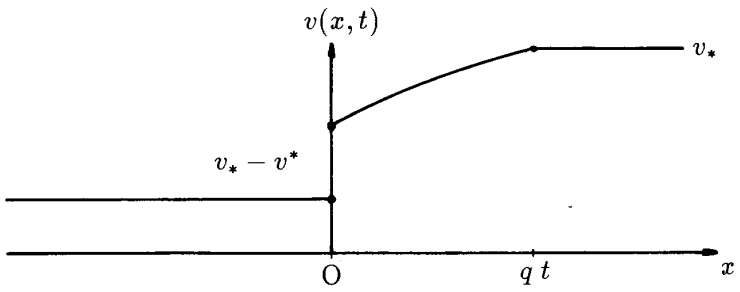

Fig 8. Crystalline solid distribution for fixed $t > 0$.

Obviously, expressions (64),(65) are only meaningful if $v > 0$. This leads us to consider the following cases.

i) $u^* = u_S(c^*)$.
This choice implies $f =$ constant $= u^*$, yielding the solution

$$u(x,t) = \begin{cases} u^* & x < qt \\ u_* & x > qt \end{cases} \tag{66}$$

and

$$v(x,t) = \begin{cases} v^* & x < 0 \\ v_* & x > 0 \end{cases} \tag{67}$$

ii) $u^* < u_S(c^*)$ and $v^* \geq u_S(c^*) - u^*$.
The second inequality being strict means that the concentration of crystalline solid is too high to be fully dissolved in the fluid. As a consequence (64) and (65) hold for all $t > 0$, where

$$v(x,t) > v(x,\infty) = \begin{cases} v^* + u^* - u_S(c^*) \geq 0, & x < 0 \\ v_* + f(x) - u_S(c^*) > 0, & 0 < x < qt. \end{cases} \tag{68}$$

iii) $u^* < u_S(c^*)$ and $v^* < u_S(c^*) - u^*$.
Now the second inequality and (65) imply that there exists a finite time $T > 0$, defined by

$$f(qT) = v^* + u^*, \tag{69}$$

such that $v(x,t) > 0$ for $0 \leq t < T$ and

$$v(x,T) = \begin{cases} 0, & x < 0 \\ v_* + f(x) - f(qT), & 0 < x < qT. \end{cases} \tag{70}$$

The distribution of the concentrations in the (x,t)-plane is sketched in Figure 9. At the point $(0,T)$ a

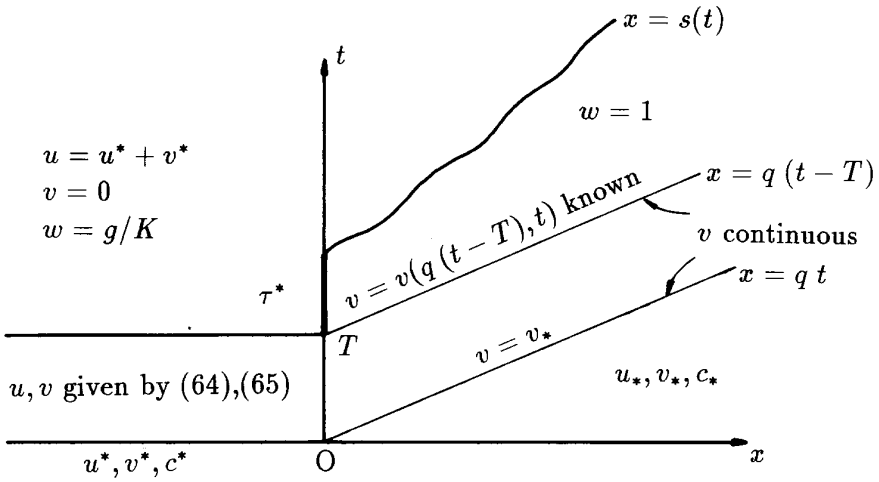

Fig 9. Concentrations in the (x,t)-plane.

dissolution front emerges as explained in Section 3.1, except that the constant v_* has to be replaced by the known function $v(q(t-T),t)$. Translating the point $(0,T)$ to the origin by setting $x = x, \tau = t - T$, and writing $s = s(\tau)$ (with $s(0) = 0$, $s(\tau) \geq 0$, for $\tau > 0$) we find the waiting time τ_*

$$\tau_* \tilde{F}(0) = v_* - v^*, \tag{71}$$

and the modified dissolution front equation (MDFE)

$$(MDFE) \begin{cases} \displaystyle\int_{\tau_*}^{\tau} \tilde{F}(s(\tau) - s(\tau_0))\, d\tau_0 = \tilde{B}(s(\tau)) \ \text{ for } \ \tau \geq \tau_*, \ \text{ where} \\ \tilde{B}(s(\tau)) = V(s(\tau)) + \tau_* \{\tilde{F}(0) - \tilde{F}(s(\tau))\} + \frac{1}{q} \displaystyle\int_0^{s(\tau)} \tilde{F}(z)\, dz. \end{cases} \tag{72}$$

In the expressions, the function $\tilde{F}$ differs from the function F used in (DFE): obviously u^* has to be substituted by $f(qT) = u^* + v^*$ in the definition of a function $\tilde{f}$ in (42) and F is given by (43) by

substituting f by $\tilde{f}$. Furthermore, the function V in $\tilde{B}$ is related to v along $x = q(t-T)$. It is found to be

$$V(s(\tau)) = v\left(s(\tau), T + \frac{s(\tau)}{q}\right) - (v_* - v^*) \tag{73}$$

or, using (65),

$$V(s(\tau)) = v^* + f(s(\tau)) - f(qT + s(\tau)). \tag{74}$$

Note that here the original function f according to definition (42) appears in (74). Clearly $V(0) = 0$. Having determined $s(\tau)$ from (71), (MDFE) and (74), one proceeds as before to find u and v in the region $s(\tau) < x < q\tau, \tau > 0$.

In principle a discontinuity of u is possible at $x = q(t-T)$. In fact u is continuous there, which can be seen as follows: Due to (64) we have $u(q(t-T)^+, t) = f(qt) = f(x + qT)$. On the other hand the definition of $\tilde{f}(x)$ leads to $u(q(t-T)^-, t) = \tilde{f}$. We have setting $h(z) = 1/(k\{K - g(z; c^*)\})$:

$$\int_{u^*}^{\tilde{f}(\delta)} h(z)\, dz = \frac{\delta}{q} + \int_{u^*}^{u^*+v^*} h(z)\, dz = \frac{1}{q}(\delta + f^{-1}(u^* + v^*)) \tag{75}$$

as $u^* + v^* < u_S(c^*)$ and thus is in the range of f. Therefore

$$\tilde{f}(\delta) = f(\delta + f^{-1}(u^* + v^*)) = f(\delta + qT) \text{ due to (69)}, \tag{76}$$

in particular we have

$$u(q(t-T)^+, t) = u(q(t-T)^-, t). \tag{77}$$

The qualitative analysis concerning dissolution fronts, as given in Section 4, is restricted to (DFE) only. This choice implies no loss of generality. All results/properties carry over to the solution of (MDFE). However, when discussing the numerical results, we do present an example in which a concentration distribution as shown in Figure 9 will arise.

4 Dissolution Front Equation

Before discussing the qualitative behavior of the dissolution front, i.e. the solution of integral equation (DFE), we recall here that this equation was derived by assuming the structural conditions (34). These conditions are consistent with the following results.

Property. Let $s : [t_*, \infty) \to [0, \infty)$ be differentiable and satisfy (DFE). Then

(i) $s(t_*) = 0$;

(ii) $\dot{s}(t_*) = q/(1 - \frac{F'(0)}{F(0)} t_* q) \in (0, q)$;

(iii) $0 < \dot{s}(t) < q$ for all $t \geq t_*$;

(iv) $s(\infty) = \infty$.

Proof (i) By assumption $s(t) \geq 0$ for all $t \geq t_*$. Since $F'(\delta) < 0$ for all $\delta \geq 0$, with $F(0) = k\{K - g(u^*; c^*)\} > 0$ and $F(\infty) = 0$, we observe that the expression B in (DFE) has the property $B(0) = 0$, $B(x) > 0$ for $x > 0$. Evaluating (DFE) at $t = t_*$ yields $B(s(t_*)) = 0$, implying at once $s(t_*) = 0$.
(ii) Differentiating (DFE) with respect to t and rearranging terms yields

$$\dot{s}(t) = \frac{F(0)}{\frac{1}{q}F(s(t)) - t_* F'(s(t)) - \int_{t_*}^{t} F'(s(t) - s(t_0))\, dt_0} \tag{78}$$

for all $t \geq t_*$. Taking $t = t_*$ in this expression and using (i) gives the desired result.
(iii) Because the right hand side in (78) is strictly positive, the lower bound is immediate. The upperbound is more involved. To show it we argue by contradiction. Thus suppose there exists $\tilde{t} > t_*$ such that

$$\dot{s}(t) < q \text{ for all } t_* \leq t < \tilde{t} \text{ and } \dot{s}(\tilde{t}) = q. \tag{79}$$

Taking $t = \tilde{t}$ in (78) and estimating

$$-\int_{t_*}^{\tilde{t}} F'(s(\tilde{t}) - s(t_0))\, dt_0 = -\int_0^{s(\tilde{t})} \frac{F'(z)}{\dot{s}}\, dz > \frac{1}{q}\left\{F(0) - F(s(\tilde{t})\right\} \tag{80}$$

results in

$$\dot{s}(\tilde{t}) < q\left\{1 - qt_* \frac{F'(s(\tilde{t}))}{F(0)}\right\}^{-1} < q. \tag{81}$$

This contradicts (79) end therefore $\dot{s}(t) < q$ for all $t \geq t_*$.
(iv) To prove this we construct a lower bound which becomes unbounded as $t \to \infty$. Let

$$C := \max_{z \geq 0}(-F'(z)). \tag{82}$$

Using this upper bound in (78) gives for $t \geq t_*$

$$\dot{s}(t) > \frac{F(0)}{\frac{1}{q}F(s(t)) + t_* C + (t - t_*)C} \geq \frac{qF(0)}{F(0) + qCt} \tag{83}$$

and after integration

$$s(t) \geq \frac{F(0)}{C} \ln\left\{\frac{1 + \frac{qC}{F(0)}t}{1 + \frac{qC}{F(0)}t_*}\right\} \tag{84}$$

This shows that $s(t)$ becomes unbounded as $t \to \infty$, see also Figure 10.

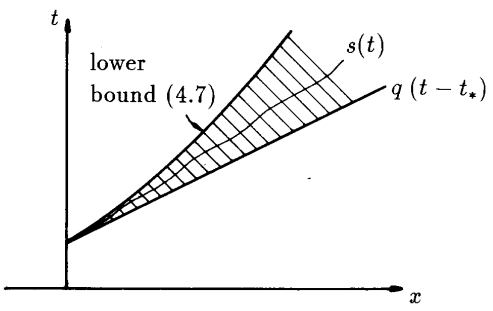

Fig 10. Estimate of location of dissolution front.

Having determined these apriori properties of the dissolution front, we now turn to the question of existence. To make use of well-known results, we transform the equation to a standard linear integral equation of the second kind for a new unknown function. Due to Property (iii), by a change of variable (see below in (91)), we can rewrite (DFE) as a linear integral equation of the first kind for the derivative of the inverse of s, denoted by τ. By differentiation, this equation transforms to

$$B'(x) = F(0)\tau(x) + \int_0^x F'(x - y)\tau(y)\, dy \text{ for } x \geq 0, \tag{85}$$

where the primes denote differentiation and where B and F are as in (DFE). In particular

$$B'(x) = \frac{1}{q}F(x) - t_* F'(x). \tag{86}$$

Equation (85) has been studied in the mathematics literature and it is known that if $F \in H^1_{\mathrm{loc}}([0,\infty))$ (i.e. F and F' are locally square integrable on $[0,\infty)$) then (85) has a unique global solution τ on $[0,\infty)$, see Zabreyko and Mayorova [8]. Furthermore, if F is continuously differentiable (in fact F is C^∞ in many relevant examples) then τ is continuous (or also C^∞) in $[0,\infty)$. As in the proof of (iii), one easily finds

$$\tau(x) > \frac{1}{q} \text{ for all } x \geq 0. \tag{87}$$

Having established the existence of a smooth function τ satisfying (85) and (87), we are now in the position to define the function $s : [0,\infty) \to [0,\infty)$ such that $s(t) = 0$ for $0 \leq t \leq t_*$ and

$$t - t_* = \int_0^{s(t)} \tau(x)\, dx \text{ for all } t > t_*. \tag{88}$$

The smoothness of τ carries over to s in $[t_*,\infty)$: for instance, if τ is continuous in $[0,\infty)$ and satisfies (87), then s is continuously differentiable satisfying (iii). Thus s is strictly increasing for $t \geq t_*$ and also $s(\infty) = \infty$ holds true due to the absence of singularities in τ. In this way, there is a one-to-one correspondence of the points $x \geq 0$ and $s(t)$ for $t \geq t_*$. To verify that the function s satisfies (DFE), we integrate (85) with respect to x from $x = 0$ to $x = s(t)$. This yields for $t \geq t_*$

$$B(s(t)) = F(0)(t - t_*) + \int_0^{s(t)} \left\{ \int_0^x F'(x-y)\tau(y)\, dy \right\} dx. \tag{89}$$

Writing

$$\int_0^x F'(x-y)\tau(y)\, dy = \frac{d}{dx}\int_0^x F(x-y)\tau(y)\, dy - F(0)\tau(x), \tag{90}$$

gives

$$B(s(t)) = \int_0^{s(t)} F(s(t)-y)\tau(y)\, dy = \int_{t_*}^t F(s(t) - s(t_0))\, dt_0. \tag{91}$$

In the last equality we used the variable transformation $s^{-1}(y) \to t_0$, as due to (88) we have $d/dy(s^{-1}(y)) = \tau(y)$. This proves the existence of a continuously differentiable dissolution front for $t \geq t_*$ which satisfies (DFE).

We conclude this section with a remark about uniqueness. Any solution of the Riemann problem (15)-(18) and (7), for which a dissolution front $x = s(t)$ according to (28) exists must be of the form discussed in Section 3 with s satisfying (DFE), provided that conditions (34) are satisfied. Now suppose two solutions are possible. They would satisfy Property (iii) and thus, using (88), one could define two solutions to the integral equation (85). But (85) has only one solution which yields a contradiction. The question arises if solutions are possible with dissolution fronts violating (34). If a solution is such that the violation occurs only after some time, i.e. there is a $t_1 > 0$ such that

$$0 \leq \dot{s}(t) \leq q \text{ for } 0 \leq t \leq t_1 \text{ and } \dot{s}(t_1) = 0 \text{ or } \dot{s}(t_1) = q, \tag{92}$$

then s satisfies the integral equation (51) in the interval $[0, t_1]$ and the waiting time t_* according to (55) exists. Assume that $t_1 > t_*$. Then the integral equation (DFE) is valid in $[t_*, t_1]$ and Property (iii) implies $0 < \dot{s}(t_1) < q$, i.e. a contradiction. Thus the only possible further solutions we cannot exclude at the moment have the very unlikely property that there are points $\hat{t}$ arbitrarily close to $t = 0$ such that $\dot{s}(\hat{t}) < 0$ or $\dot{s}(\hat{t}) > q$.

5 Numerical method and results

In this section we construct numerical solutions of the Riemann problem (15)-(18) and (7). The numerical solution procedure is based on the method of characteristics and follows the lines of Section 3 in detail. We shall give quantitative results for two distinct non-equilibrium cases:

i) The crystalline solid is only present in the flow domain where $x > 0$, i.e. $v^* = 0, v_* > 0$

ii) The crystalline solid is initially present everywhere in the flow domain, i.e. $v^*, v_* > 0$

The parameters used in the computations are adopted from Willis and Rubin [6] and listed in Table 1. The differences are the following: K is slightly larger, in Willis and Rubin [6] only the equilibrium case $k = \infty$ is considered. K is determined by c_{1*} and c_{2*} and thus has to be different from Willis and Rubin [6], as we do not consider Debye-Hückel corrections in our computations. But note that also these could be handled without problems as the rate function is of general form. The value of fluid concentration c_1^* used in our computations differs from the value given in the caption of Figure 3 in Willis and Rubin [6]. The value in the caption is $c_1^* = (\mathrm{Sr}^{2+})_f = 2.0\mathrm{x}10^{-5}$ mMol/cm^3 (which we used in Part I) while Figure 3 suggests that the correct value used by Willis and Rubin [6] equals $c_1^* = 2.0\ \mathrm{x}10^{-4}$ mMol/cm^3. We decided to use the latter value in this paper.

$$
\begin{array}{lcrl}
\Theta & = & 0.32 & \\
\rho & = & 1.8 & [\mathrm{g/cm^3}] \\
q^* & = & 0.3\mathrm{x}10^{-3} & [\mathrm{cm/s}] \\
M_1 & = & \mathrm{Sr}^{2+} & \\
M_2 & = & \mathrm{SO}_4^{2-} & \\
n & = & 1 & \\
m & = & 1 & \\
c^* & = & 2.0\mathrm{x}10^{-4} & [\mathrm{mMol/cm^3}] \\
c_* & = & 0.0\mathrm{x}10^{-4} & [\mathrm{mMol/cm^3}] \\
k_p & = & 1 & \\
k_d & = & K & = 3.8688\mathrm{x}10^{-7} \\
k & = & 0.1 & [1/\mathrm{s}] \\
c_{12*} & = & 4.9\mathrm{x}10^{-5} & [\mathrm{mMol/g}] \\
c_{12}^* & = & 0.0\mathrm{x}10^{-5} & [\mathrm{mMol/g}] \\
c_1^* & = & 2.0\mathrm{x}10^{-4} & [\mathrm{mMol/cm^3}] \\
c_{1*} & = & 6.22\mathrm{x}10^{-4} & [\mathrm{mMol/cm^3}]
\end{array}
\qquad (93)
$$

Table 1. Parameters used in the computations.

5.1 Numerical method

The numerical procedure consists of the following steps: evaluation of integral (42) to obtain a numerical approximation of the function $f(\delta)$, substitution of $f(\delta)$ in (43) to obtain $F(\delta)$, numerically solving a Volterra integral equation which follows from (DFE) to find the location of the dissolution front $s(t)$ and finally we go back to (41) and (42) to determine u. The concentration of the crystalline solid is obtained by integration of (37).

The integrand of (42) becomes singular when u^* tends to the solubility concentration $u_S(c^*)$. This singularity has to be handled with care because we need numerical approximations of $f(\delta)$ in a wide range of δ values. We used Clenshaw-Curtis quadrature in combination with symbolic transformation techniques to remove the singularity, as implemented in the computer algebra system Maple, see Geddes [2]. The result of the numerical integration is given as a table $[\delta_i, f(\delta_i))]$, where $\delta_i = i \cdot \Delta\delta$. Only in special cases, i.e. $n = 1, m = 0$ (the linear case) and $n = m = 1$, exact evaluation of integral (42) is possible. We used the exact expressions (45),(48) to verify the accuracy of the numerical integration of (42). The discrete result of (42) is used to evaluate (43), i.e. $F(\delta_i)$ on the δ-grid.

Equations (85),(86) can be written as a standard linear Volterra integral equation of the first kind, i.e.

$$\tau(\delta) = h(\delta) - \int_0^\delta K(\delta - y)\ \tau(y)\ dy \tag{94}$$

where

$$h(\delta) = \frac{1}{q}\frac{F(\delta)}{F(0)} - t_* \frac{F'(\delta)}{F(0)} \tag{95}$$

and kernel

$$K(\delta - y) = \frac{F'(\delta - y)}{F(0)}. \tag{96}$$

We solve this equation explicitly, using the trapezoidal rule to discretize the integral in (94). The approximation of the derivatives are chosen central in δ, except in the first integration step where the derivatives are discretized forward in δ. The position of the dissolution front follows from the definition of τ, hence

$$t - t_* = \int_0^{s(t)} \tau(z)\ dz. \tag{97}$$

Because τ is computed at the location of the grid points we have $s(t) = i\Delta\delta$ and the corresponding value of t is found by approximating the right hand side of (97) using Simpson's rule. To compute a profile of the fluid concentration u at a certain time level t_1 we choose a point $\mathrm{P}(y, t_1)$ in the (x,t)-plane (see Figure 11). We walk backwards along the characteristic through point P and compute the coordinates of the

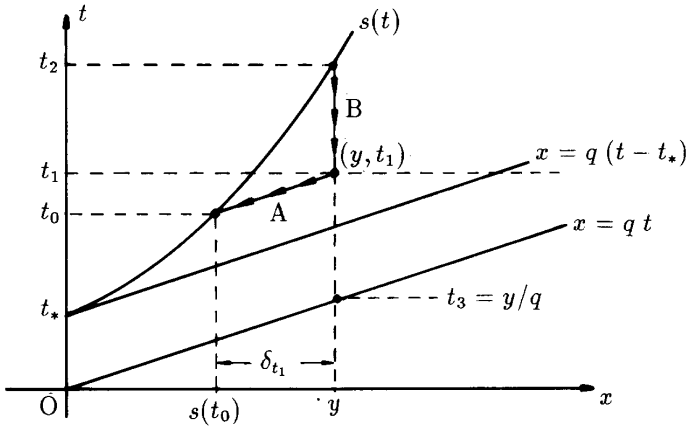

Fig 11. Construction of solutions in the (x,t)-plane.

intersection point $(s(t_0), t_0)$ of the characteristic and the free boundary curve $s(t)$. The precise procedure is as follows: start in point P, follow the characteristic in the direction of the dissolution front $s(t)$, check in every grid point if the t-coordinate of the characteristic is above the corresponding t-coordinate of $s(t)$ in that point. If this is the case we use the last and before last step to compute the intersection point of the characteristic and $s(t)$, assuming that the approximation of $s(t)$ is piecewise linear between successive coordinates. This gives the desired value $\delta_{t_1} = y - s(t_0)$, corresponding to point P. Next we use

the table of discrete $[\delta_i, f(\delta_i)]$-values to compute the fluid concentration $u(y,t_1) = f(\delta_{t_1})$ in P. Because δ_{t_1} (usually) does not coincide with one of the δ_i-values in the table, we have to interpolate once more. A fluid concentration profile is constructed by repeating this procedure in the region $s(t_1) \leq y \leq q\,(t_1 - t_*)$ at a sufficiently large number of points P.

To obtain a numerical approximation of the concentration v of the crystalline solid in point $\mathrm{P}(y,t_1)$ we first have to obtain values of the fluid concentration in discrete points along the vertical line through (y,t_2) and (y,t_1) using the procedure given above, see line B in Figure 11. By explicit integration in time of (37) from the position of the free boundary, i.e. t_2 to the position of P, i.e. t_1, we obtain $v(y,t_1)$. Full integration from the position of the free boundary $(s(t_2),t_2)$ to the position of the fluid front (y,t_3) has to reproduce the boundary condition v_* (up to a small error, due to the discrete numerical approximations), which follows from (51). This serves as a check for the accuracy of the numerical procedure. For the linear case $(n = 1, m = 0)$ we compared results obtained by the numerical procedure and the corresponding exact solutions and found excellent agreement.

5.2 Results

In this section we give computed results for the following cases:

1. The linear case $n = 1, m = 0$ for $v^* = 0$
2. A non-linear case $n = 1, m = 1$ for $v^* = 0$ and for $v^*, v_* > 0$
3. A non-linear case $n = 2, m = 2$ for $v^* = 0$.

Remark: In order to obtain comparable time, space and concentration scales for all cases considered in this section we introduce an artificial factor a that multiplies the function g and assume $K = 3.8688\text{x}10^{-7}$ to be independent of the values of n and m. This implies that only the results of the computations for the case $n = m = 1$ have physical meaning. The values of a used in the computations are:

n	m	a
1	0	$6.22\text{x}10^{-4}$
1	1	1.0
2	2	$1.83\text{x}10^{+6}$

The linear case: n=1,m=0.
Figure 12 shows the position of the crystal dissolution front in the (x,t)- plane for the linear case $(n = 1, m = 0)$. In this example we have $t_* = 10499$s. The dissolution front is a straight line which satisfies exactly expression (62). Due to the introduction of a we have to replace kt_* by akt_* in the denominator of (62). Figure 13 shows breakthrough curves of the fluid concentration at different observation points. An observation independent of this special case is: There are horizontal parts in these curves, which

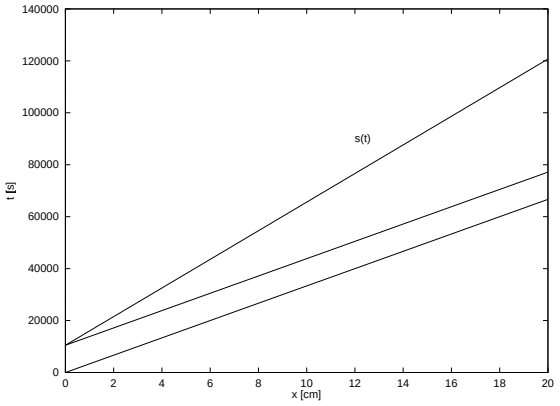

Fig 12. Dissolution front in the (x,t)-plane for the linear case.

correspond to the fluid concentration in the region in the (x,t)-plane where $x_1/q \leq t \leq x_1/q + t_*$ at a

given position $x = x_1$. In this region $\delta = x_1$ is constant and therefore u is constant, $u = f(x_1)$ increasing monotonically form u^* to $u_S(c^*)$ for x_1 ranging from 0 to ∞. The width of the flat region in all curves is constant and equal to the waiting time t_*. Figure 14 shows the time evolution of the crystalline solid concentration at different positions. The regions with constant slope in the v-curves correspond to the regions in the breakthrough curves for u where u is constant.

Figure 15 gives profiles of the fluid concentration at different time levels. We observe several points in the u-profiles where the derivative $u_x = \partial u/\partial x$ is discontinuous. The discontinuity in u_x at the toe of the profiles in Figure 15 travels with speed $\dot{s}(t)$. A simple computation shows that for the general case

$$\frac{\partial}{\partial x}u(s(t)^+, t) = k\{K - g(u^*; c^*)\}\ \frac{1}{q - s'(t^-)} \tag{98}$$

The second discontinuity (from the left) in u_x reflects the discontinuity of $\dot{s}(t)$ at $t = t_*$. Its position is

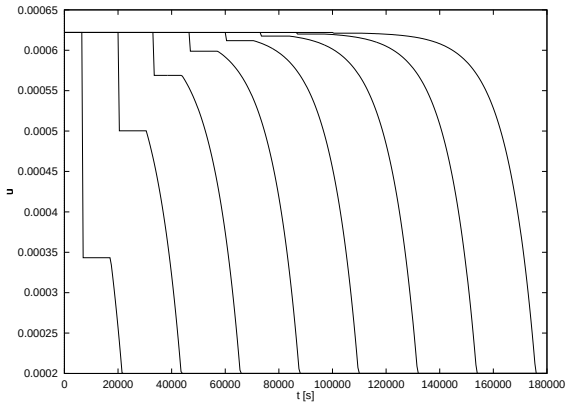

Fig 13. Breakthrough curves of the fluid concentration u at different positions for the linear case. From left to right the observation points are: x = 2,6,10,14,18,22,26 and 30 cm. (See Figure 12)

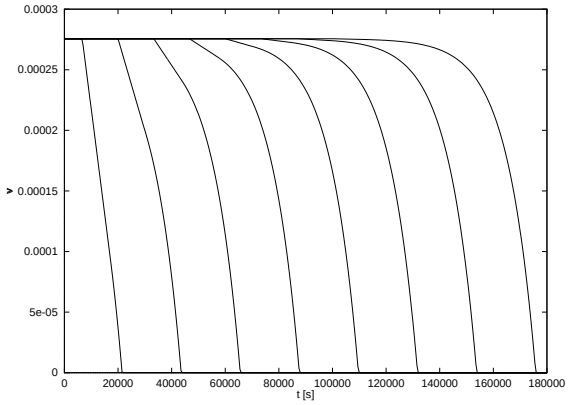

Fig 14. Time evolution of the crystalline solid concentration v at different positions for the linear case. From left to right the observation points are: x = 2,6,10,14,18,22,26 and 30 cm. (See Figure 12)

a point at the line $x = q(t - t_*)$ in the (x,t)-plane for a given time t. In fact, we have in general due to Property (ii) for such (x,t)

$$\frac{\partial}{\partial x}u(x^+, t) - \frac{\partial}{\partial x}u(x^-, t) = -f'(x)\ \frac{1}{kt_*\frac{\partial}{\partial u}g(u^*; c^*)} \tag{99}$$

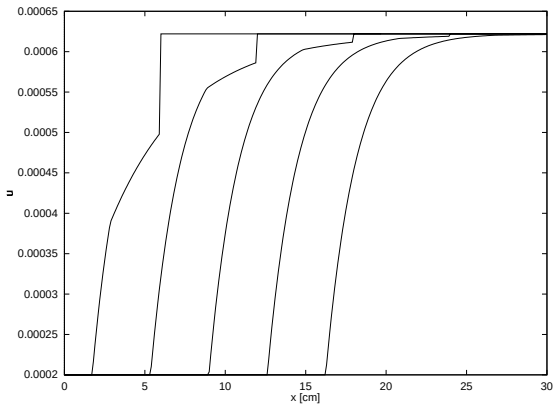

Fig 15. Fluid concentration profiles at different time levels for the linear case. From left to right the curves correspond to $t = 20000,40000,60000,80000,100000$ s. (See Figure 12)

At the fluid front, i.e. the top of the u-profile, we have a jump in u which is consistent with the Rankine-Hugoniot shock condition (27), and given by

$$u(qt^+,t) - u(qt^-,t) = u_* - f(qt) \to u_* - u_S(c^*) < 0 \tag{100}$$

An exception is the linear case, as here $u_S(c^*) = u_S(c_*) = u_*$ and thus the discontinuity at $x = qt$

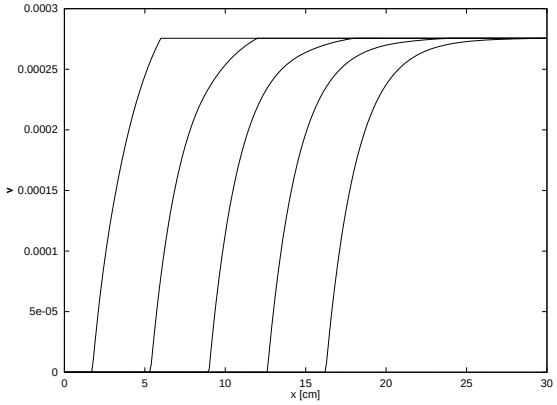

Fig 16. Crystalline solid concentration profiles at different time levels for the linear case. From left to right the curves correspond to $t = 20000,40000,60000,80000,100000$ s. (See Figure 12)

vanishes for $x_1 \to \infty$. Figure 16 shows the corresponding profiles of v. The derivative $v_x = \partial v/\partial x$ at the dissolution front is discontinuous, due to the discontinuity in u at the front. The constant speed is given according to (62) by

$$\dot{s}(t) = \frac{q}{1+kt_*} = \frac{u^* - u_*}{u^* - u_* + v^* - v_*} q \tag{101}$$

which corresponds to the speed of travelling waves, which exist for constant c (compare Part 1, in particular (54)). By inspection of the explicit solution given by (101), (63), (40), (45) for the Riemann problem and the explicit solution for the travelling wave problem (note that g is independent of c here) derived from Part 1, (94),(54) we see that for taking the shift $L = at_*$, where a is given by (101), the solutions coincide for $x < (t - t_*)q$. In particular there is pointwise convergence in x for $t \to \infty$ of the solution profile here to the travelling wave solution.

A non-linear case: n=1,m=1

For this case we shall distinguish between the two sets of initial and boundary conditions as discussed in Section 3.1 and Section 3.2.

Crystalline solid only partly present (See Section 3.1)

In this case the solubility concentration is given by $u_S(c) = \frac{c}{2} + \frac{1}{2}\sqrt{c^2 + 4K}$, i.e. $u_S(c^*) > u_S(c_*) = u_*$. We have chosen $c^* = u^* = 2.0\text{x}10^{-4}$ and because $c_* = 0$ we have $K = u_*(u_* - c_*) = u_*^2$, see Table 1. For the waiting time t_* we find 7108.0 s. The dissolution front $s(t)$ is now a curve with slope $\dot{s} < q$ for all $t \geq 0$. Figure 17 shows the position of the dissolution front in the (t, x)-plane. The curve suggests that

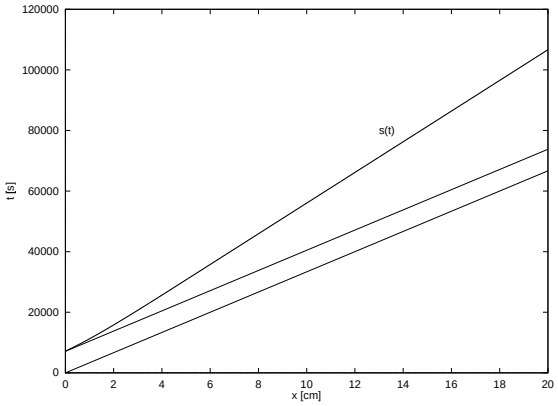

Fig 17. Dissolution front in the (x, t)-plane for the non-linear case $n = m = 1$.

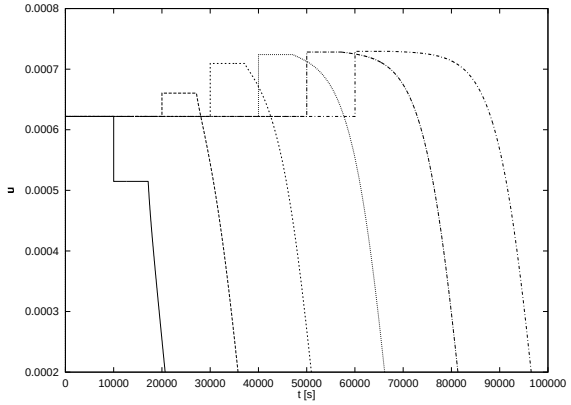

Fig 18. Breakthrough curves of the fluid concentration at different positions for the non-linear case $n = m = 1$. The observation points are x = 3.0,6.0,..,18.0 cm. (See Figure 17)

$\dot{s}(t_*) = q$ which is not true. In fact the $\dot{s}(t_*)$ satisfies Property (ii) in Section 4 where in this example it turns out that $F'(0)/F(0)t_*q << 1$. Figure 18 shows breakthrough curves of u for different observation points. The qualitative differences as compared to the linear case are the following: i) The toe of the u-profile does not travel with constant speed but with speed $\dot{s}(t)$. ii) After a certain time the maximum concentration in the profiles exceeds u_* and increases in time to the solubility concentration $u_S(c^*)$. iii) The fluid concentration at the fluid front remains discontinuous and jumps either from below or from above to u_*. Figure 19 gives the corresponding curves for v. The properties of the time evolution of the crystalline solid concentration compare to the those in the linear case, see Figures 14 and 19. Figure 20 shows the fluid concentration profiles at different time levels for the non-linear case. The corresponding crystalline solid concentrations are given in Figure 21.

A quantitative comparison between the solutions of the Riemann problem for the non-linear case and the solutions found by Willis and Rubin [6] is not possible because they allow for diffusion in their problem and consider only equilibrium reaction. Comparing Figure 3, Figure 20 and the corresponding general

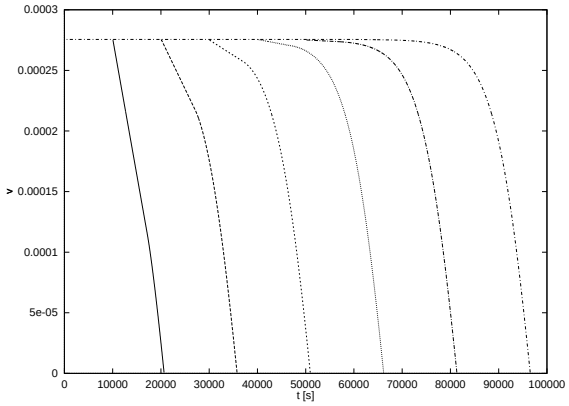

Fig 19. Time evolution of the crystalline solid concentration at different positions for the non-linear case $n = m = 1$. The observation points are x = 3.0,6.0,..,18.0 cm. (See Figure 17)

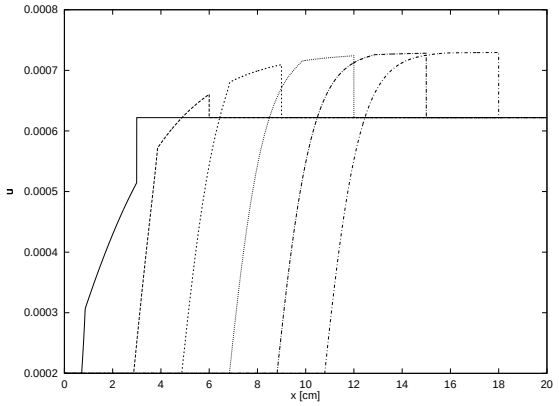

Fig 20. Fluid concentration profiles at different time levels for the non-linear case $n = m = 1$. From left to right the curves correspond to t = 10000.0,20000.0,.., 60000.0 s. (See Figure 17)

statements mentioned and Figure 3 of Willis and Rubin [6] indicates: The common qualitative property caused by the interplay of transport and dissolution is a "plateau-structure", which for a fixed time t is defined by the spatial intervals $I_1 = \{x|x < s(t)\}$, $I_2 = \{x|s(t) < x < qt\}$,$I_3 = \{x|x > q)\}$. In I_3 the solution is given by the "initial condition" $u_* = u_S(c_*)$, in I_1 by the "boundary condition" $u^* = u_S(c^*)$ and in I_2 at least asymptotically, i.e. for large t, by $u_S(c^*)$. The piece-wise constant structure of Figure 3 without dispersion and kinetics is smeared out by the addition mechanisms in different ways. Kinetics leads to a smoothing effect in I_2 such that the transition at $x = s(t)$ becomes continuous and the maximum is attained at $x = qt$. Diffusion smooths more, effecting also I_1 and I_3 and leading to overall smooth and nonconstant profiles, where the maximum in I_2 is attained at $x = s(t)$. The solutions for other values of n and m have properties that compare to the solutions of the non-linear example discussed in this section.

Crystalline solid present everywhere. (See Section 3.2)

Two characteristic times arise in this case: T = 2680 s, which is the time needed to dissolve all initially present crystalline solid ($v^* = 1.0\ 10^{-4}$) in the region $x < 0$ and τ_* = 4903 s, which is the waiting time for the dissolution front. For $t \geq T$ we have $u = u^* + v^* = 3.0\text{x}10^{-4}$ in the region $x < 0$. Figure 22 shows

the position of the dissolution front in the (x,t)-plane. Figure 23 gives breakthrough curves of u and

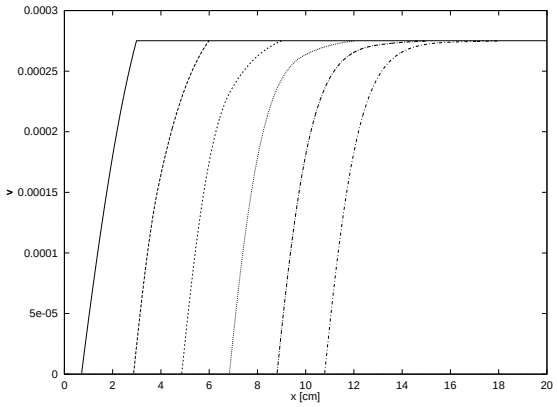

Fig 21. Crystalline solid concentration profiles at different time levels for the non-linear case $n = m = 1$. From left to right the curves correspond to t = 10000.0,20000.0,.., 60000.0 s. (See Figure 17)

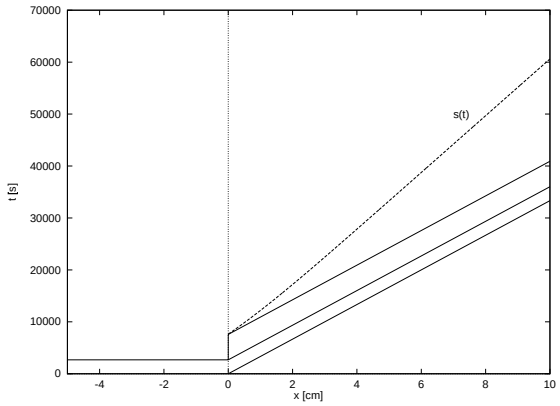

Fig 22. Dissolution front in the (x,t)-plane for the case $n = m = 1$, $v^*, v_* > 0$. (Compare with Figure 9).

the time evolution of v at different positions in one graph. The upper set of curves is u and the lower is v. The horizontal parts in the u-curves have width τ_* and give rise to linear parts in the v-curves, while the increasing parts, which vanish as time proceeds, have width T. The crystalline solid concentration along the line $x = q(t - T)$ in the (x,t)-plane is known and given by (65). We used this to check the accuracy of the computations.

A non-linear case: n=2, m=2

For any combination of $n, m \geq 1$ the function $g(u; c^*)$ is monotonically increasing and convex in the interval $c/m \leq u \leq u_S(c^*)$ and there for we may expect similar qualitative behavior of the solutions. The position of the dissolution front in the (x,t)-plane is shown in Figure 24. Now the solubility concentration is given by $u_S(c) = c/4 + \sqrt{c^2 + 16\sqrt{K/a}}/4$. The factor a is chosen such that $u_S(c) = 7.299\text{x}10^{-4}$, as in the case $n = m = 1$. The breakthrough curves of u are given in Figure 25 and the corresponding time evolution of v in Figure 26.

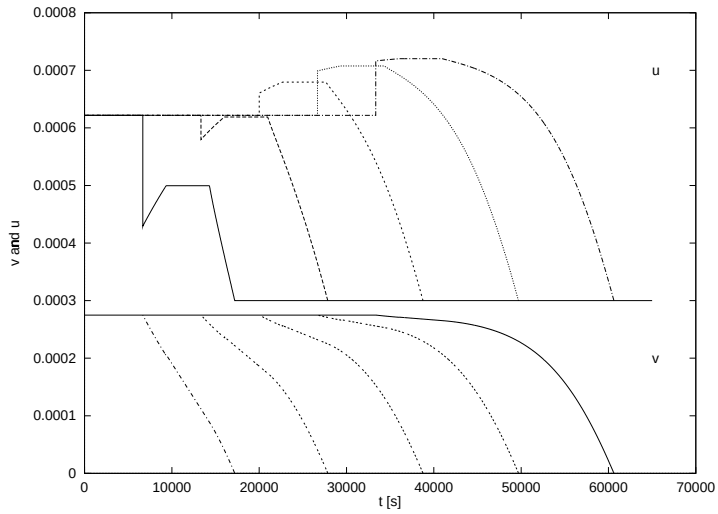

Fig 23. Breakthrough curves of u (upper curves) and time evolution of v (lower curves) at positions $x = 2, 4, 6, 8, 10$ cm for the non-linear case $n = m = 1$, $v^*, v_* > 0$.

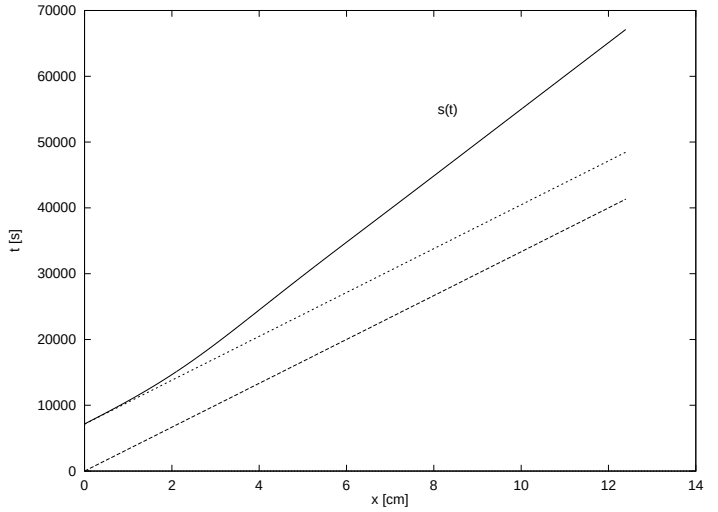

Fig 24. Dissolution front in the (x, t)-plane for the case $n = m = 2$, $v^* = 0$

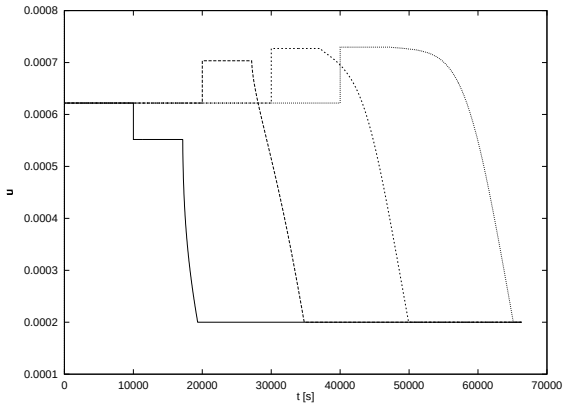

Fig 25. Breakthrough curves of u at $x = 3, 6, 9$ and 12 cm for the case $n = m = 2$, $v^* = 0$.

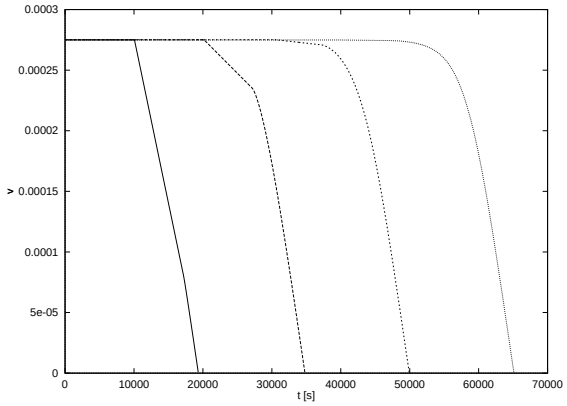

Fig 26. Time evolution of v at $x = 3, 6, 9$ and 12 cm for the case $n = m = 2$, $v^* = 0$.

6 Conclusions

We considered a model for transport and dissolution/precipitation, where the kinetics of the reaction is taken into account, but diffusion/dispersion is ignored. The appearance and evolution of a dissolution front from corresponding initial states, i.e. the Riemann problem of the hyperbolic system, is investigated. The initial states for the "charge distribution" c are "incompatible" in general, i.e. the "ionic composition" of the fluid changes. The method of characteristics leads to a nearly explicit representation of the solution, where only an implicitly defined function f (42) has to be evaluated numerically and based on f an integral equation (61) has to be solved numerically (or rather the transformed equation (85),(86)). The basic "plateau-structure" of the solution is revealed being characterized by the dissolution front $x = s(t)$ with speed less than q, where (for non-equilibrium) $\partial u/\partial x$ and $\partial v/\partial x$ are discontinuous and the fluid or salinity front $x = qt$, where u and $\partial v/\partial x$ are discontinuous. A comparison of solutions elucidates the role of kinetics and of diffusion/dispersion, which turns out to be similar, but in detail different mechanisms. In addition, due to non-equilibrium, the dissolution front s only starts to move after a positive time t_*, with positive slope, which implies a discontinuity in $\partial u/\partial x$ at $x = q(t - t_*)$. Because of these properties the solutions are principally different from the travelling wave solutions of Part 1 for "compatible" boundary conditions and only local convergence can be expected for $t \to \infty$.

References

[1] Bryant, S.L., Schechter, R.S. & Lake, L.W., Mineral Sequences in Precipitation/Dissolution Waves, *AIChE Journal* **33** (1987), pp 1271-1287.

[2] Geddes, K.O., Numerical Integration in a Symbolical Context, In: B. Char (ed.), *Proceedings of SYMSAC'86*, ACM Press (1986), pp 185-191.

[3] Knabner, P., Van Duijn, C.J. & Hengst, S., An analysis of crystal dissolution fronts in flows through porous media. Part 1: Compatible boundary conditions, *Advances in Water Resources*, Vol **18**, No 3 (1995), pp 171-185.

[4] LeVeque, R.J., Numerical Methods for Conservation Laws, Birkhäuser Verlag, Basel, 1992.

[5] Schweich, D., Sardin, M. & Jauzein, M., Properties of Concentration Waves in Presence of nonlinear Sorption, Precipitation/Dissolution, and Homogeneous Reactions 1. Fundamental, *Wat. Res. Res.* **29** (1993), pp 723-733.

[6] Willis,C. & Rubin, J., Transport of Reacting solutes subject to a moving dissolution boundary: Numerical methods and solutions., *Water Resour. Res.* **23** (1987), pp 1561-1574.

[7] Whitham, G.B., Linear and Nonlinear Waves, Wiley, New York, 1974.

[8] Zabreyko, P.P. & Mayorova, N.L., Integral Equations-A Reference text, Noordhoff Int. Publ., Leiden, 1975.